Influence of electrical boundary conditions on molecular dynamics simulations of ionic liquid electrosprays

Arnaud Borner,* Pengxiang Wang, and Deborah A. Levin†
Department of Aerospace Engineering, The Pennsylvania State University, University Park, Pennsylvania 16802, USA
(Received 30 May 2014; published 2 December 2014)

Molecular dynamics (MD) simulations are coupled to solutions of Poisson's equation to study the effects of the electrical boundary conditions on the emission modes of an electrospray thruster fed with an ionic liquid. A comparison of a new tip boundary condition with an analytical model based on a semihyperboloidal shape offers good agreement, although the analytical model overestimates the maximum value of the tangential electric field since it does not take into account the space charge that reduces the field at the liquid surface. It is found that a constant electric field model gives similar agreement to the more rigorous and computationally expensive tip boundary condition at lower flow rates. However, at higher mass flow rates the constant electric field produces extruded particles with higher Coulomb energy per ion, consistent with droplet formation. Furthermore, the MD simulations show that ion emission sites differ based on the boundary condition and snapshots offer an explanation as to why some boundary condition models will predict emission in a purely ionic mode, whereas others suggest a mixed ion-droplet regime. Finally, specific impulses and thrusts are compared for the different models and are found to vary up to 30% due to differences in the average charge to mass ratio.

DOI: 10.1103/PhysRevE.90.063303 PACS number(s): 02.70.−c, 94.05.−a, 52.65.−y, 47.57.−s

I. INTRODUCTION

Electrospray thrusters, characterized by their small size, low power consumption, high specific impulse, and low thrust are one possible type of propulsion technology that can be used for small satellites [1–3]. Typically, electrospray thrusters use an ionic liquid (IL) as the fluid, which is transported from a reservoir to an emitter, usually to a capillary-type emitter [4–7] or an externally wetted or porous emitter [8–10]. When a potential difference is applied between the emitter and an extractor, high electric (E) fields are generated and deform the liquid surface to create a Taylor cone [11]. A jet is emitted from the tip of the Taylor cone to form the cone-jet structure [12,13]. In the case of electrosprays, the cone-jet usually operates in a mixed ion-droplet mode [14,15] or pure ion mode (PIR) [16,17], depending on the type of propellant used, in the case of interest here, an IL. ILs are attractive as propellants for electric propulsion because of their low volatility and high electrical conductivity, as well as their *green* properties. Moreover, imidazole-based ionic liquids have been investigated in terms of dual-mode chemical monopropellant and electrospray rocket propulsion capabilities and found to be attractive candidates [18].

A number of groups have studied the physics of colloid thrusters with electrohydrodynamic approaches [19,20] using explicit assumptions to model the behavior of the fluid or molecular dynamics (MD) approaches [21–24] that focus on the microscopic properties of ILs and the evaporation of ions from droplets. However, these approaches either do not provide enough information regarding the physics of formation of Taylor cones or consider groups of large droplets, which are not representative of propulsive devices. As in our previous work [25–27], this study uses a coarse-grained (CG) potential to model the IL 1-ethyl-3-methyl-imidazolium tetrafluoroborate (EMIM−BF_4) interactions in molecular dynamics simulations. This approach has been found to decrease the computational costs of these nonequilibrium simulations by orders of magnitude compared to all-atom models for similarly sized systems. Note that the recently introduced coarse-grained model of Merlet *et al.* [28] for EMIM−BF_4 and BMIM − BF_4 may offer additional computational savings because the $EMIM^+$ cation is represented by three interaction sites in contrast to the four sites used by Ref. [29]. The effective-force coarse-grained (EFCG) model of Wang *et al.* [30] is used in this work, where the $EMIM^+$ cation is represented as four interaction sites respectively labeled M1, IM, MR, and M2, while the BF_4^- anion is represented as a single interaction site.

In addition, a number of laboratory measurements on EMIM−BF_4 IL electrosprays have been made [4–7], further making it a good candidate for fundamental MD studies. Ryan *et al.* [31] studied the flow rate sensitivity to voltage across four electrospray modes for three liquids, including EMIM−BF_4. They found that in the absence of any flow control mechanism, the influence of electrostatic pressure in driving that flow is the key process in the voltage-driven electrospray. Other recent experiments emphasize the need to study the minimum flow rate required to obtain cone-jet stability [32,33]. However, none of the computational or experimental studies on electrospray thrusters offer any information on the behavior and magnitude of the electric field inside the device. Of special interest are the effects of the applied mass flow rate on the local structure of the electric field. This is necessary in order to fully understand how the microscopic behavior of the ions affect the propulsive properties of electrospray thrusters.

In our previous work [26], different cone-jet structures were obtained for a constant electric field, e.g., Taylor cone, cone-jet structure, and multijet structure at high field strengths. However, in order to fill the gap created by the absence of information regarding the nature of the electric field during ion emission, we improved our model to account for the induced

*arnaud.p.borner@nasa.gov
†deblevin@illinois.edu

electric field due to space charge repulsion by coupling our MD simulations to a three-dimensional Poisson solver [27]. The modeling of space charge, however, introduces significant numerical considerations such as grid cell size, electrical boundary conditions (BC), and longer computational times. The grid cell size was varied such that spatial convergence was obtained with computational times for the coupled MD-Poisson simulations on the order of several hundreds of picoseconds. The electrical boundary conditions, especially at the tip of the capillary, were investigated in detail. The "plate" and "needle" BCs were proposed and the values of the potential and electric fields, when both Laplace's and Poisson's equation were solved, were computed and compared. It was found that the needle BC generated very large potential gradients in the vicinity of the capillary tip, producing unrealistically high radial electric fields. The maximum in the tangential electric field (the direction parallel to extrusion) was localized slightly off the tip of the capillary, and the maximal value was found to be similar to earlier theoretical [12] and numerical predictions [34–36]. When currents were computed, however, both BCs behaved differently. The plate BC underestimated all current values but the ratios of ion and droplets to total current were similar to experiment [4]. As the extraction voltage was increased, the monomer current became the largest constituent of the total current, largely because an increase in the extraction potential caused an increase in the electric field values, which extracted more non-solvated ions from the liquid meniscus. In the case of the needle BC, all currents matched the experimental values [4] closely at low mass flow rates but showed a discrepancy a higher flow rate values. We believe this is due to the manner in which the boundary conditions were defined and the proximity between the capillary tip and the domain boundary.

For these reasons, an improved boundary condition that is numerically accurate and comparable with earlier analytic results is considered in this work. First, the "tip" BC is introduced as an evolution of the needle BC and the electric fields and currents that it predicts are compared with the earlier BCs. Furthermore, the electric field for the tip BC is compared with that obtained for a simplified model for the tip of an electrospray capillary with a liquid Taylor cone, representing it as a hyperboloid surface. Using the different boundary conditions, the MD simulations are analyzed in terms of the average Coulomb energy per extruded ion, emission modes, and propulsion characteristics. It is found that for low mass flow rates the simple, constant electric field model provides good agreement with experiment at a much lower computational cost. However, at high mass flow rates, it diverges from the more rigorous tip BC and experiment because it predicts too high a monomer current.

II. NUMERICAL APPROACH

In all the MD simulations presented in this work, 9455 EMIM−BF_4 ion pairs are placed inside a Pt capillary composed of 16 626 atoms. To treat this large a system for time periods long enough to establish steady-state currents a coarse-grained model is used instead of a full atomistic description. In the case of EMIM−BF_4, four particles represent the $EMIM^+$ ion (two methyl groups, a CH_2 group, and the imidizolium group, respectively, named M1, M2, MR, and IM), and only one particle is used to model the BF_4^- ion. The system size was chosen as a compromise between the computational cost and the minimum capillary diameter with a cylinder height to radius ratio of about five to preserve the capillary needle shape. The inside radius and length of the capillary were taken to be respectively 56 and 275 Å, so the initial density of the system following equilibration was the same as the measured value of 1240 kg/m^3 at 295 K. Interactions between the IL and the Pt atoms were modeled by simple Lennard-Jones 12-6 interactions in a one-zone model [37,38]. During the extrusion, the IL temperature inside the capillary was maintained by means of a Langevin thermostat [39] and, following previous work [26,27], a similar time step of 5 fs was again used in this work, since we concluded that it provided the same accuracy as smaller time steps with a lower computational cost [26]. No periodic boundary conditions were applied during the extrusion.

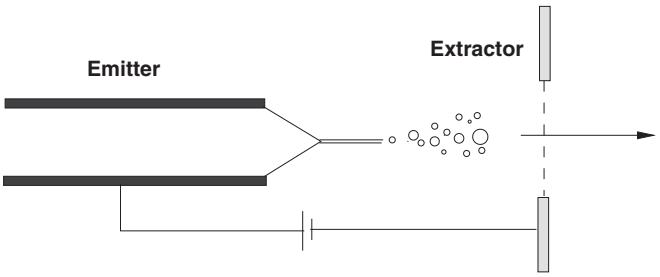

FIG. 1. Single emitter colloid thruster.

A Poisson solver was developed to simulate the plasma between the capillary tip and a planar electrode for the generic single emitter geometry shown in Fig. 1. A typical particle-in-cell (PIC) solver has four modules: field solver, particle mover, and two interpolation modules for weighting of particles to the field, and inverse weighting of the electric field back on to the particles. In this work the particle mover is replaced by the MD software DL_POLY [40]. At each time step, after the inter- and intramolecular interactions are calculated by DL_POLY, the positions of all charged particles are passed to the Poisson solver. The field solver solves for the electrostatic field with space charges based on the gradient of the potential, which is obtained by solving the Poisson equation,

$$\nabla \cdot \nabla \phi = -\frac{\rho_f}{\epsilon}. \tag{1}$$

on a Cartesian grid that is single level and of uniform spacing. The solver is based on the finite-difference approach in which the governing equation, Eq. (1), is discretized as follows:

$$\frac{\phi_{i+1,j,k} - 2\phi_{i,j,k} + \phi_{i-1,j,k}}{(\delta x)^2} + \frac{\phi_{i,j+1,k} - 2\phi_{i,j,k} + \phi_{i,j-1,k}}{(\delta y)^2} + \frac{\phi_{i,j,k+1} - 2\phi_{i,j,k} + \phi_{i,j,k-1}}{(\delta z)^2} = -\frac{\rho_f}{\epsilon}, \tag{2}$$

where i, j, k are indexes in the x, y, z directions and δx, δy, and δz are the cell lengths in the x, y, and z directions, respectively. The values of the coefficients of the left-hand side of Eq. (2) form a square matrix of dimension equal to the number of grid points with the unknown variables, ϕ, forming the unknown vector. The linear matrix system is solved for the

unknown vector in terms of the right-hand side of Eq. (2) using the generalized minimal residual method (GMRES) [41].

Once values of the potential are obtained across the domain, the electrostatic field is computed for each grid point. The calculated electrostatic field is interpolated back from the grid points to the particle locations to compute the forces acting on the particles. In this work, first-order interpolation (linear weighting) [42] is used to carry out charge and field interpolation. The electric field at each particle location is passed back to DL_POLY and the forces on the particles are calculated in the MD software as

$$\vec{F} = q\vec{E}, \tag{3}$$

where q is the charge associated with a particle and $\vec{F}$ and $\vec{E}$ are the force and the field vectors, respectively. The electric field is calculated from the potential, ϕ, which is obtained by solving the Poisson equation [Eq. (2)],

$$\vec{E} = -\vec{\nabla}\phi. \tag{4}$$

The IL particles are then moved across the domain using the forces calculated for each of the particles and the MD simulation advances to the next time step. While the influence of the grid size was studied previously [27], it is interesting to note that the cell size was picked to be similar to the cutoff for the computation of long-range electrostatic (Coulomb) interaction, 25 Å. Therefore, any electrostatic interaction at a distance less than the cell size was modeled by the MD force calculation, while any interaction at a distance larger than 25 Å was modeled by the Poisson solver. This treatment ensures that the cell size does not have to be chosen to be on the order of the Debye length, which is under an angstrom in the Taylor cone and therefore not computationally achievable (time- and memory-wise). It should be noted that the Wolf sum [43] was used to calculate the electrostatic interactions between ions, as opposed to the Ewald sum, which computes a real and imaginary part of the interaction, since the use of the Ewald summation is restricted to 3D periodic systems in DL_POLY.

To predict the suitability of cone jets as colloid thrusters, important propulsive parameters such as the thrust and specific impulse or efficiency can be calculated directly from the atomistic simulations. The specific impulse, I_{sp}, and thrust, T, are given by

$$I_{sp} = \frac{u'}{g}, \tag{5}$$

$$T = \dot{m} I_{sp} g, \tag{6}$$

where u' is the average velocity of the extruded charged cluster in the direction of extrusion at the extraction ring, g is gravity's acceleration, and $\dot{m}$ is the mass flow rate.

III. INFLUENCE OF BOUNDARY CONDITIONS

Two sets of BCs for the computational domain were investigated in previous work [27]. The first one, labeled as plate BC and shown in Fig. 2(a), consists of grounding ($V = 0$ V) the entire surface around the capillary (Dirichlet BC). The second one, labeled as needle BC and shown in Fig. 2(b), consists of grounding the surface of the capillary

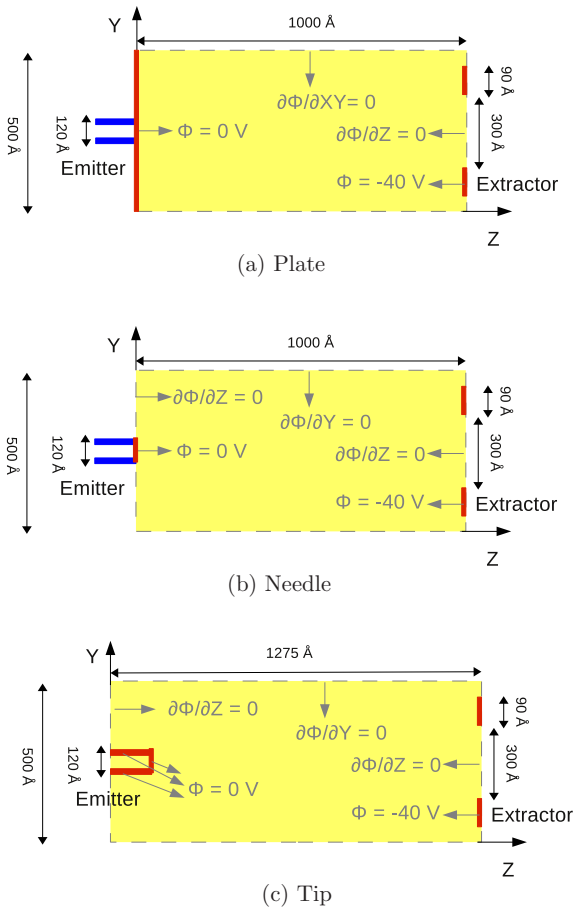

FIG. 2. (Color online) Cross section of the computational domain in the YZ plane showing the boundary conditions.

(a circle of radius 56 Å) with a Dirichlet BC and using a Neumann BC ($E_Z = 0$) on the area around the capillary on that surface. In both cases, a Neumann BC is used on all other faces, except on the extraction ring that has a radius of 300 Å and a radial thickness of 90 Å and where a Dirichlet BC is applied with a potential of −40 V.

A third boundary condition is introduced here, which will be labeled a "tip BC." Figure 2(c) shows a sketch of the tip BC. It is similar to the needle BC, but the capillary is introduced inside the computational domain and its entire cylindrical surface is grounded. The computational domain is therefore extended by 275 Å in the Z direction. Figure 3 shows a comparison of the electric field in the Y (lateral or radial) direction for the needle (left) and tip (right) BCs in the absence of any electrospray ions for the solution of Laplace's equation [Eq. (1) with $\rho_f = 0$]. It can be seen that the highest value of the radial electric field occurs on the side of the capillary in a region that we will show does not contain cations that are emitted from the capillary. In contrast, the needle BC has much larger radial fields than the tip BC which we will show significantly changes the MD predictions of the IL flow. Examination of the electric field for the needle BC on the left side of Fig. 3 shows that the discontinuity in the boundary condition overestimates the radial electric field at the edge of the capillary, and, as will be shown in the MD simulations, effectively pulls the ions radially

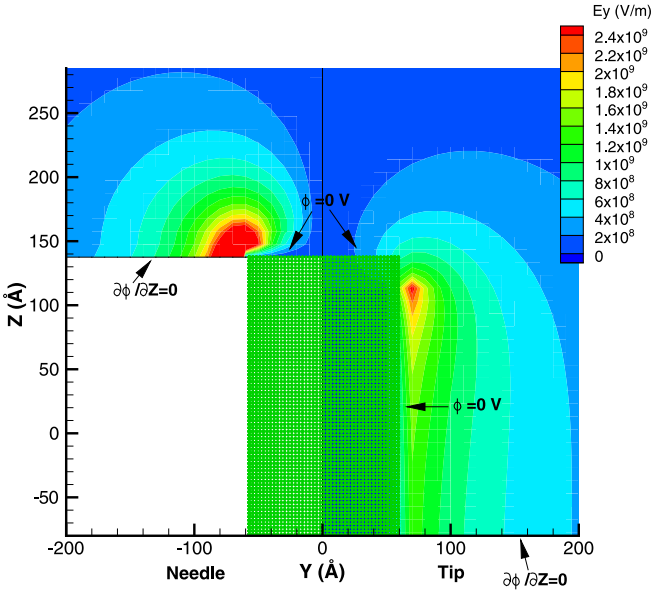

FIG. 3. (Color online) Comparison of the radial (Y direction) electric field for Laplace's equation for the needle (left) and tip (right) BCs, with an extraction voltage of −40 V. The green rectangle centered at (0;69) represents the location of the capillary.

outwards from the capillary rather than in the predominantly tangential direction as might seem desirable from the point of view of enhancing thrust. Figures 4(a) and 4(b) show the spatial distribution of the potential and tangential electric field for the tip BC, again assuming that there are no cation particles in the domain. The region of maximum tangential electric field is a circle of radius 60 Å centered around the axis of the cylinder.

In order to validate our tip BC model further, it was compared with the electric field produced when the boundary condition was modified so the grounded volume was a semi-hyperboloidal tip rather than a cylinder. Martinez-Sanchez proposed a simplified model for the tip of an electrospray capillary with a liquid Taylor cone, representing it as a hyperboloid surface [12]. His simple model showed that for any IL the current could be related to its viscosity, conductivity, and the mass flow rate through the capillary. Figures 5(a), 5(b), and 5(c) show the spatial distribution for the potential and radial and tangential electric fields, respectively, in the absence of any charged particles for a hyperboloid shape grounded to 0 V relative to the extractor ring and fully inside the computational domain, similarly to the tip BC of the cylindrical capillary. The main difference between the Laplace solutions for the tip and hyperboloid models is that the red area that represents the region with the highest tangential electric field is concentrated at a single grid point for the hyperboloid [Fig. 5(c)], as opposed to a line with two edges of higher value for the tip BC [Fig. 4(b)]. However, when extrusion begins in the MD simulation EMIM−BF_4 particles are introduced into the domain and, as seen on Fig. 6, the region of highest tangential field is now moved across the liquid meniscus, in the semicircle of particles above the capillary, demonstrating good spatial agreement with Martinez-Sanchez's model. Since the latter does not take into account space charge, and it is known that the space charge acts to reduce the field at the liquid surface, it comes as no surprise that the maximum value of the electric field in the hyperboloid model [Fig. 5(c)] in the absence of any charged particles overestimates the value obtained from the coupled MD-Poisson simulation for the tip BC (Fig. 6).

IV. INFLUENCE OF MASS FLOW

The effect of the mass flow on the behavior of the cone jet as well as currents has been studied previously [26,27] and it was hypothesized that the induced electric field should have an effect on the stability of the jet. In our previous work, good agreement with experiments was often observed at the lowest mass flows, but a sharp increase in the monomer current at high mass flow rates during the transient part of the extrusion led to an overestimation of the total current. Currents are computed

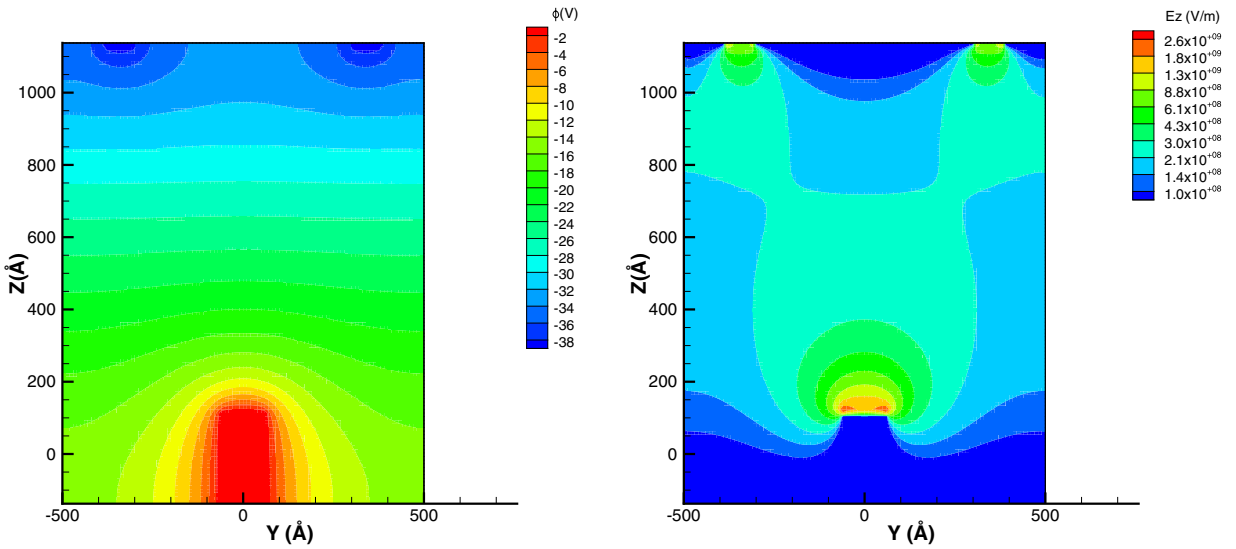

(a) Potential (b) Tangential E field

FIG. 4. (Color online) Potential and tangential electric field distributions with no particles, for the tip BC, with an extraction voltage of −40 V.

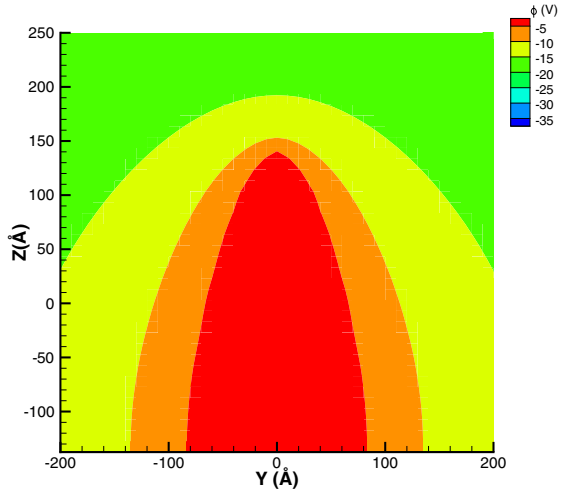

(a) Potential

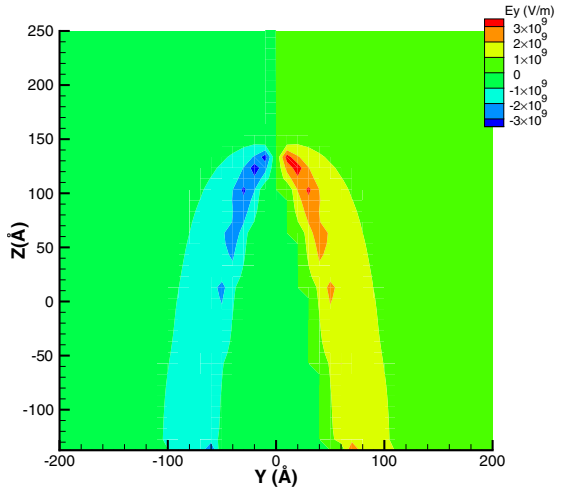

(b) Radial E field

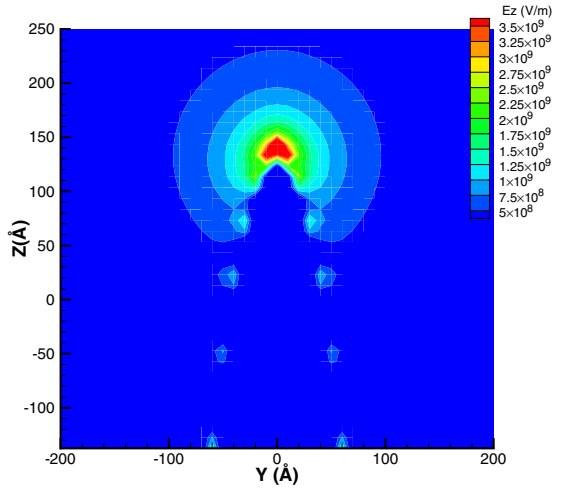

(c) Tangential E field

FIG. 5. (Color online) Zoomed-in view of the potential, radial, and tangential electric field distributions when Laplace's equation is solved, for a semihyperboloidal boundary condition, with an extraction voltage of −40 V. The boundary between the red and orange contours in Fig 1(b) represents the location of the grounded semihyperboloidal surface (in black-white printed version, the boundary is located between the darker shade of grey at the center of the picture and the neighboring medium dark grey).

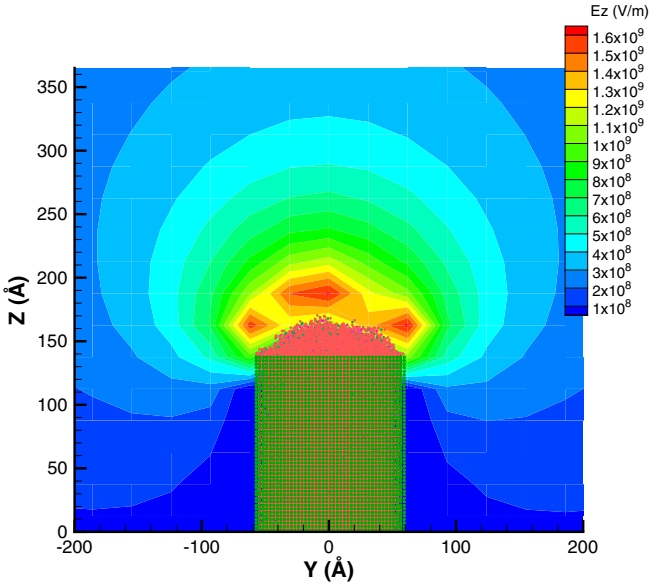

FIG. 6. (Color online) Zoomed-in view of the tangential (Z direction) electric field when Poisson's equation is solved, for the tip BC, with an extraction voltage of −40 V. Green spheres represent Pt capillary atoms and red spheres the $EMIM^+$ ions, whereas purple spheres represent BF_4^- ions (in black-white printed version, the light grey rectangle centered at (0;69) represents the Pt capillary and the darker meniscus on top of it represents the IL).

from the MD simulations as the ratio of the number of charges crossing the extractor plane per time interval, and are expressed as cumulative moving averages, in order to prevent sharp fluctuations in the current values as a function of time. In this work, the time interval is chose to be 1000 time steps or 5 ps. All current values reported in subsequent tables were averaged over 100 ps after steady state was reached for cation emission.

In Figs. 7(a) and 7(b), a comparison between the currents computed at −40 V for the new tip BC, a constant electric field of 0.4 V/nm in a similar fashion as in Ref. [26], and the values measured by Romero-Sanz [4] can be observed. It can be seen that the tip BC agrees well with the trends from Romero-Sanz, although our computed values underestimate the experimental values. The authors point out that the starting voltage or distance between capillary and extractor ring are unknown for Romero-Sanz's experiments, making it hard to assess whether the ratio of applied voltage to starting voltage was the same for the experiments and our model. The major trends from the experimental results of increasing then decreasing monomer current, uniformly increasing dimer current, mainly constant trimer current, and slowly increasing droplet current as a function of IL mass flow rate are replicated by the tip BC. Note that in this work, droplets are defined as positively charged entities comprised of nine or more ions. Also the constant electric field model offers close agreement with the tip BC and experimental values for lower mass flow rates but diverges from those results at higher mass flow rates where it overpredicts the experimental current by about 50%, mainly due to a large overprediction in the monomer current. The constant electric field model tends to overestimate the droplet current and droplet size, due to the fact that the field predicted by that model in the vicinity of the liquid meniscus

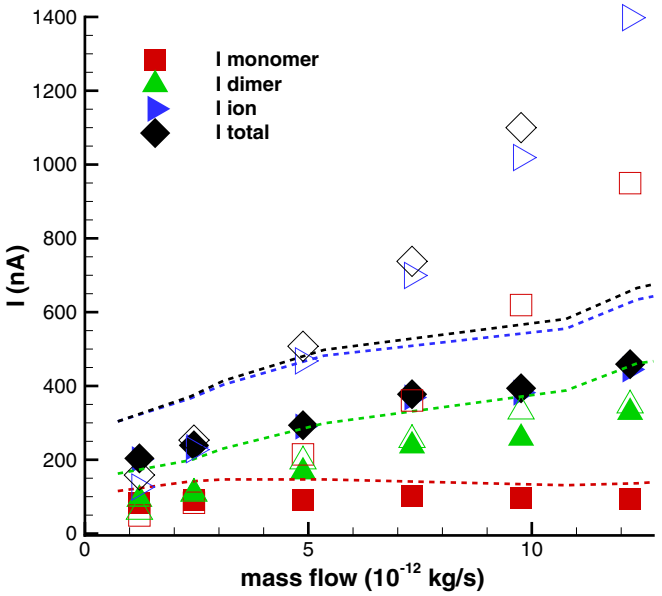

(a) Monomer, dimer, ion and total currents

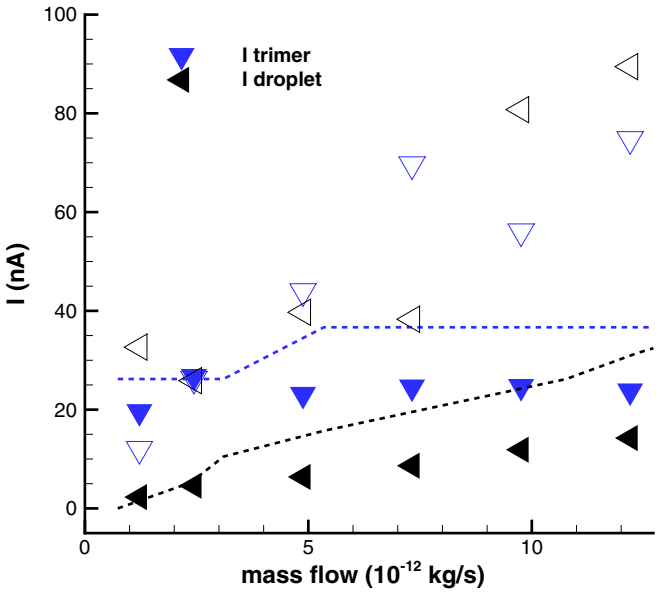

(b) Trimer and droplet currents

FIG. 7. (Color online) Currents as a function of the mass flow rate. Filled symbols represent the currents with the tip BC for an extraction potential of −40 V, empty symbols represent the currents for a constant electric field of 0.4 V/nm and dashed lines represent the measured current values from Romero-Sanz *et al.* [4].

is underestimated. This can be seen by comparing the constant E-field value of 0.4 V/nm to values larger than 1.0 V/nm for the tip BC shown in Fig. 6. The computational cost of the tip BC model versus the constant electric field is about 5 to 6 times larger with the grid size presented in the results ($40 \times 40 \times 51$ mesh with a cell size of 25 Å), mainly due to the operations necessary in inverting large matrices when solving Poisson's equation. In 24 CPU h on 8 Intel Xeon X5675 six-core, 3.06-GHz processors, the MD simulation of the constant electric field case of 0.4 V/nm with an applied mass flow of 2.44×10^{-12} kg/m^3 moves forward about 500 ps, whereas for the tip BC case for an extraction potential of −40 V and similar mass flow rate the MD-coupled Poisson calculation advances only 107 ps. This raises the question of whether the coupled MD-Poisson tip BC model is worth the computational cost increase when compared to the constant electric field model used in MD and how they compare with experimental results. As simplified as the constant electric field is, i.e., with no change in the electric field since space charge is ignored, constant in time, and only directed in tangential direction, it still provides results that are comparable with those of the more extensive tip BC for a fraction of the computational cost and is not sensitive to computational parameters such as the grid size or boundary conditions. However, in the next section we show that the predicted IL spray characteristics and system quantities such as currents and thrusts differ for the two models.

V. COMPARISON OF MOLECULAR STRUCTURES FOR DIFFERENT BOUNDARY CONDITIONS

As a way to better understand the influence of the boundary conditions on the behavior of the ionic liquid electrospray system, the potential energy of the system, i.e., ions in the capillary and extruded ions, was compared for different boundary conditions. Of the two components to the intermolecular potential, Lennard-Jones and Coulomb, it was found that only the latter interaction varied significantly throughout the MD simulation time and as a function of the BC model. Figure 8 shows the Coulomb energy of the entire electrospray system as a function of time for four different models: a constant electric field of 0.3 V/nm, a one-dimensional (1D) electric field model uncoupled to the MD simulation and similar to the one derived in Ref. [27] for a potential of −30 V, and

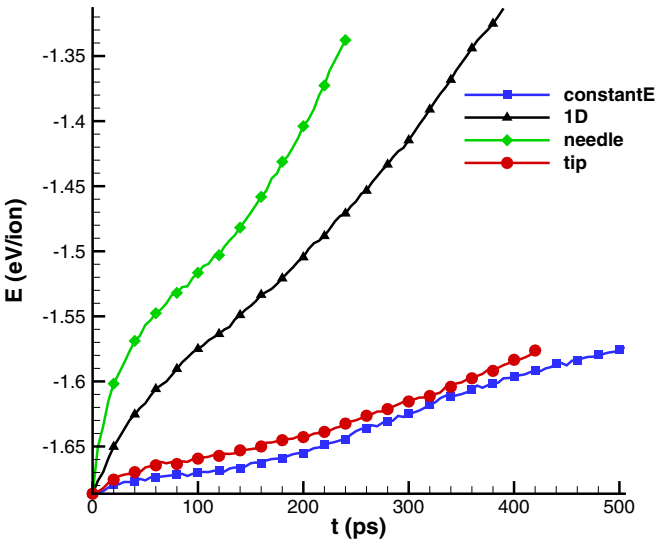

FIG. 8. (Color online) Normalized Coulomb energy of the entire electrospray system as a function of time for four different models: a constant electric field of 0.3 V/nm, a 1D electric field model similar to the one derived in Ref. [27] for a potential of −30 V, and the needle and tip BCs for an extraction potential of −30V. The total number of ions in the electrospray system is 18 910.

TABLE I. Average Coulomb energy, estimated specific impulse, and thrust for different models for a mass flow rate of 2.44×10^{-12} kg/s.

Model	Energy/ion (eV/ion)	I_{sp} (s)	T (mN)
Constant E field 0.3 V/nm	−0.95	368	8.8
1D E field −30 V	−0.55	478	11.4
Needle BC −30 V	−0.6	465	11.1
Tip BC −30 V	−0.4	397	9.5

coupled MD-Poisson simulations of the needle and tip BCs for an extraction potential of −30V. Two distinct groups can be extracted from the plot: the needle BC and 1D electric field model behave similarly, as do the constant electric field model and tip BC. Since the 1D electric field was derived based on Laplace's solution of the needle BC, it comes as no surprise that the two models behave similarly. On the other hand, the agreement between the simplest model, the constant electric field model, and the high-fidelity coupled MD-Poisson tip model cannot be explained as easily.

To remove the influence of the ions inside the capillary on the average Coulomb energy, a second type of calculation was performed. First, the Coulomb energy of ions that are inside the capillary is computed at the initial time, prior to extrusion with a value of −1.68 eV per ion inside the capillary obtained. Then, at each time step, the number of ions inside and outside the capillary were recorded so the total Coulomb energy of the system could be computed. The total number of extruded ions varied from 1652 to 6518, depending on the extrusion time which was model dependent. A simple calculation leads to the average energy per extruded ions which is shown in Table I for each model. Again, the needle BC and 1D electric field model shows similar results for the aforementioned reason. On the other hand, while the constant electric field model and tip BC showed similar trends in Fig. 8, it can be seen that the average Coulomb energy of their extruded particles differs substantially. This is due to the fact that the constant electric field model predicts a higher droplet current and large droplets as can be seen in the top left portion of Fig. 9. Since the Coulomb energy is simply a measurement of long-range electrostatic interactions between ions, the large difference can be explained by the fact that large droplets of over 20 ions will significantly increase the absolute value of the total Coulomb energy. For the same reason, ions inside the capillary (nonextruded ions) have a higher absolute value of the average Coulomb energy per ion, since these ions have a large number of neighbors in the capillary where the density is high.

Figure 9 shows visual snapshots of the behavior of the different boundary conditions and models, as well as zoomed-in views. The constant electric field model is shown to visually operate in a mixed ion-droplet mode where droplets are emitted as products from the cone-jet breakup. The 1D electric field and needle BC models are both shown to operate in an almost purely ionic mode. The MD snapshots show that the main difference in the two models is the emission point of the ions, i.e., in the 1D electric field model, most ions are emitted from the tip of the Taylor cone, resulting in a jet with a spread angle on the order of approximately a dozen degrees, while in the case of the needle BC, ions are emitted from any location

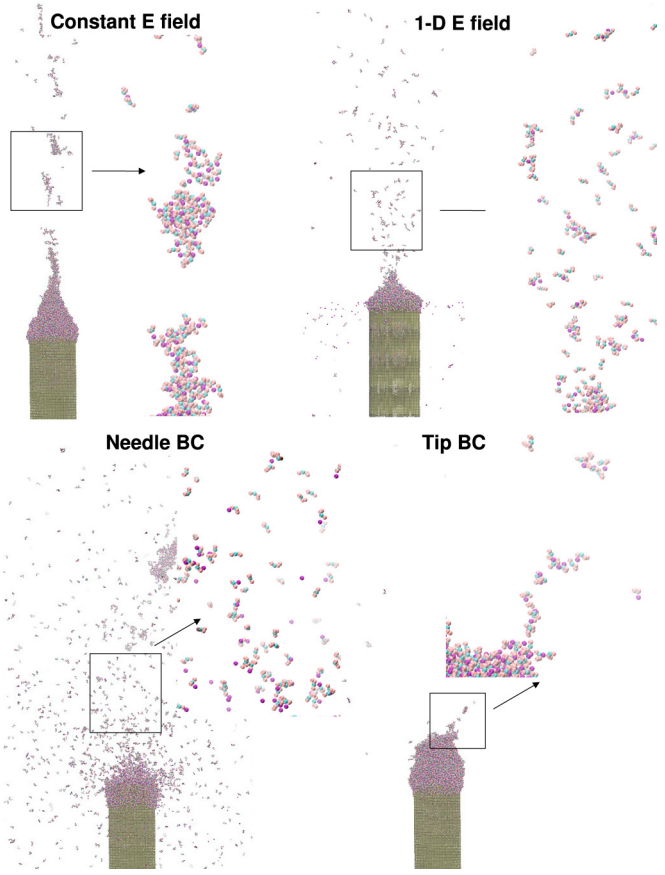

FIG. 9. (Color online) Spatial distribution of the IL for different boundary conditions and models, with a mass flow rate of 2.44×10^{-12} kg/s and an extraction potential of −30 V (except for the constant electric field that was 0.3 V/nm). The Z scale is 1275 Å. There are 9455 ion pairs in each simulation.

at the tip of the capillary and no Taylor cone is visually discernible, leading to a cloud of nonsolvated ions and no clear collimated plume. Finally, in the case of the tip BC, a mixture of predominantly ions and some droplets is emitted from a conical looking meniscus, and charges are emitted not only from the tip of the meniscus but also in the immediate vicinity.

Figure 10 shows zoomed-in snapshots of two droplets generated with the constant electric field and tip BC models. In the case of the constant electric field, the droplet encounters multiple Coulomb fissions that reduce its partial charge from +6 to +1 as it travels away from the emitter. Of the three snapshots in the first row of Fig. 10, the droplet is located approximately 500 Å away from the emitter on the first snapshot and about 900 Å away on the last one. For the case of the tip BC, the second row of Fig. 10, the droplet is located closer to the emitter, between 70 and 300 Å, and is oriented perpendicularly to the direction of extrusion. In the two subsequent snapshots it spatially reorients itself in the direction of extrusion since further away from the emitter the tangential electric field is much larger than the radial field, as can be seen when comparing the right-hand side of Figs. 3 and 4(b). On the centerline ($X = Y = 0$ Å) at $Z = 250$ Å, the tangential electric field is over two orders of magnitude larger than the radial field (5.4×10^8 versus 2.1×10^6 V/m).

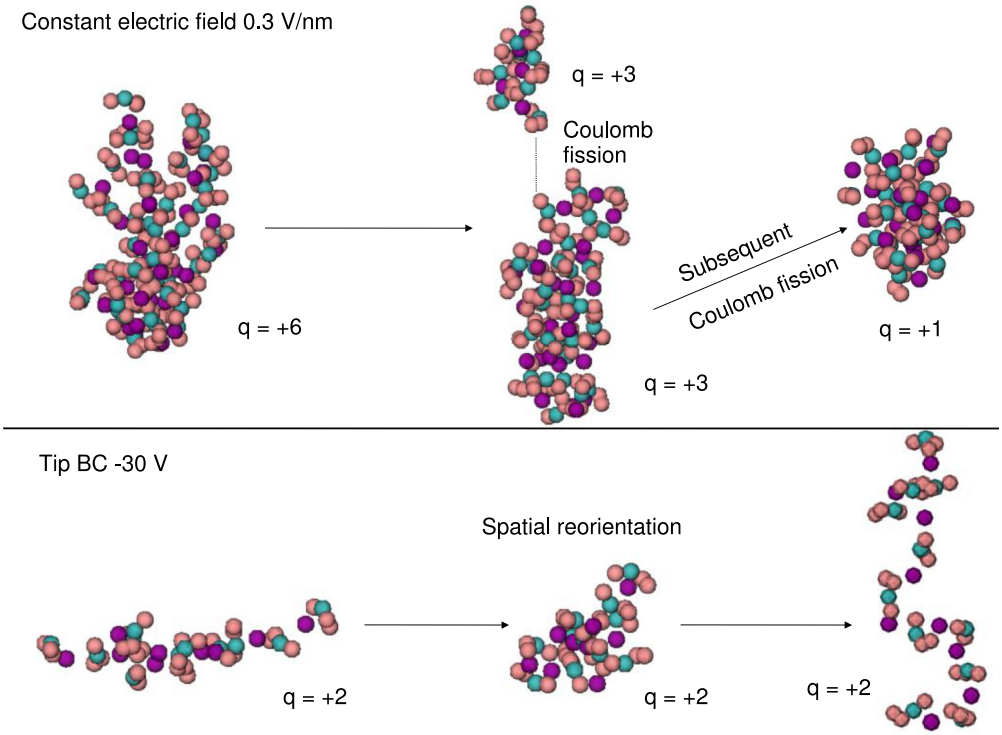

FIG. 10. (Color online) Zoomed-in snapshots of droplets generated by the constant electric field model for a field of 0.3 V/nm and the tip BC with an extraction voltage of 0.3 V/nm. Green spheres represent Pt capillary atoms; red spheres represents M1, MR, and M2 groups; green-blue spheres represent the IM groups, and purple spheres represent BF_4^- ions (in black-white printed version, spheres in lighter shades of grey represent groups part of the cation while darker shades of grey represent the BF_4^- ion). The Z axis points up (similar to Fig. 9) and its scale is 36 Å.

The reorientation of the droplet is similar to the ion-cage structure deformation reported by Shi and Wang [44] at high electric fields, since the self-diffusion of ions along the electric field becomes faster than the other two directions due to the anisotropic deformation of ion cages.

VI. DEPENDENCE OF PROPULSION BEHAVIOR ON BOUNDARY CONDITION

Turning to the analysis of currents and thrust, Table II shows the different currents for the aforementioned four models for a mass flow rate of 2.44×10^{-12} kg/s. The currents are averaged values over 100 ps after steady state is reached for the emission. The 1D electric field model and needle BC generate total currents that are unreasonably high because the monomer current is larger than that of dimers. The currents obtained when using the tip BC at −30 V are significantly lower than those obtained with the constant electric field model at 0.3 V/nm, while they were comparable for an extraction potential of −40 V and a constant electric field of 0.4 V/nm. This result shows that the constant electric field model is less sensitive than the tip BC model to input parameters such as the extraction voltage. As a comparison, when the electric field was reduced from 0.4 to 0.3 V/nm, the total current was reduced by 20%, while it was reduced by 70% when the extraction voltage was reduced from −40 to −30 V for the tip BC.

Finally, the thrust and specific impulse predicted by the MD simulations for each of the four models are summarized in Table I. Depending on the model and boundary conditions,

TABLE II. Currents for different models and the experimental values from Romero-Sanz *et al.* [4] for a mass flow rate of 2.44×10^{-12} kg/s.[a]

Model	Monomer	Dimer	Trimer	Ion	Droplets	Total (nA)
Constant E field 0.3 V/nm	21.1%	33.5%	8.8%	64.6%	35.4%	202.6
1D E field −30 V	65.6%	31.5%	4.2%	99.8%	0.2%	777.6
Needle BC −30 V	56.1%	33.6%	7.4%	99.1%	0.9%	445.3
Tip BC −30 V	29.4%	46.7%	12.7%	90.6%	9.4%	76.9
Romero-Sanz [4]	29.5%	60.0%	7.4%	96.8%	3.2%	380
Constant E field 0.4 V/nm	33.0%	42.7%	10.4%	89.8%	10.2%	253.3
Tip BC −40 V	37.9%	45.8%	11.2%	98.1%	1.9%	239.1

[a]All currents are in percentages of the total current, which is expressed in nA.

the specific impulse values range from 368 to 478 s and the corresponding thrust values range from 8.8 to 11.1 nN for a mass flow rate of 2.44×10^{-12} kg/m^3 and an extraction potential of -30 V (or the corresponding electric field of 0.3 V/nm). As can be expected from the currents and average Coulomb energy per ion, the 1D and needle models give similar results and higher specific impulse and thrust than the constant electric field and tip models. This is because the former have a larger contribution to the total currents from monomers (Table II) that reach a higher velocity when extruded due to their lower q/m, where q is the ion or droplet charge and m is its mass.

VII. CONCLUSION

Molecular dynamics simulations have been coupled to a 3D Poisson solver to study the effect of boundary conditions on the emission modes of an IL-colloid-thruster flow. Four boundary conditions and models were studied, including a proposed new model based on an embedded tip inside the MD computational domain. It was found that the different boundary conditions and the manner in which they are coupled or uncoupled from the MD simulations have a significant impact on the behavior of the electrospray system. The needle BC was observed to generate large potential gradients in the vicinity of the capillary tip, producing radial electric fields that were unrealistically large and therefore emitting ions with a much larger spread angle than expected. Comparison of the fields and atomistic simulations generated by the new tip and needle BCs showed that the former eliminated that artifact. The electric fields generated by the tip BC were also compared with a semihyperboloidal model that has been used to derive a number of analytic relationships of thruster current to fundamental IL properties such as conductivity and viscosity. The tip BC offered good spatial agreement with the semihyperboloidal model, although the latter overestimates the maximum value of the tangential electric field since it does not take into account the space charge that reduces the field at the liquid surface.

The influence of the four different models on predicted charged species currents and as a function of mass flow rate was studied. While previous boundary conditions, such as the plate and needle, do not follow the experimental trends reported by Romero-Sanz [4] at high mass flow rates, the tip BC predicts good qualitative agreement throughout the entire mass flow rate range, although it slightly underestimates the currents values. The seemingly simple, computationally cheaper, constant electric field model gives similar agreement to the more rigorous tip BC at lower flow rates but it diverges from both the tip BC and experiment when the mass flow rate increases because it predicts too high a monomer current. Additionally it was found that the constant electric field model was less sensitive to input parameters such as the extraction potential. Comparison with experiment is often hampered by the fact that the extrusion voltage is not reported so the constant electric field may be a good approximation but it should be verified that the MD simulation predicts the correct jet emission mode.

Analyses of the MD simulations shows that the manner of extrusion and the average Coulomb energy per ion depend on the boundary conditions and the degree of coupling between the electric field and the MD simulation. It was found that the energy per extruded ion was similar for the 1D electric field and the needle BC conditions as was found for current species distributions as a function of mass flow rate. Unlike the earlier comparisons, however, this diagnostic explained why the constant electric field model produces more droplets than the tip BC. Comparison of the emission modes predicted by the MD simulations also change depending on the BC. The 1D electric field and needle BC models are both shown to operate in an almost purely ionic mode, whereas the constant electric field and the tip BC emit both ions and droplets with the latter emitting fewer droplets. It was found that droplets emitted from the tip BC elongated in similar fashion to the ion-cage deformation previously reported [44] when placed in a constant electric field applied in only one direction. Finally, specific impulses and thrust were computed for the different models and compared, and models that predict the highest total current also predicted higher specific impulses and thrusts (by 30%), due to the differences in the average charge-to-mass ratio. The authors recommend use of the tip BC as the most general approach with additional investigations into improving its computational efficiency.

ACKNOWLEDGMENTS

The research being performed at the Pennsylvania State University was supported by the Air Force Office of Scientific Research through MACEEP Grant No. FA9550-09-1-0695, whose support is gratefully acknowledged. The authors are grateful to Professor John Daily for providing the DL_POLY [40] tabulated potential input file and fruitful discussions.

[1] V. E. Krohn, Progress in Astronautics and Rocketry **5**, 73 (1961).
[2] V. E. Krohn, Jr., Prog. Astronaut. Aeronaut. **9**, 435 (1963).
[3] J. Mueller, Prog. Astronaut. Aeronaut. **187**, 449 (2000).
[4] I. Romero-Sanz, R. Bocanegra, J. Fernandez de la Mora, and M. Gamero-Castaño, J. Appl. Phys. **94**, 3599 (2003).
[5] Y. Chiu, B. Austin, R. Dressler, D. Levandier, P. Murray, P. Lozano, I. Katz, J. de la Mora, and M. Sanchez, J. Propul. Power **21**, 416 (2005).
[6] D. Garoz, C. Bueno, C. Larriba, S. Castro, I. Romero-Sanz, J. Fernandez de La Mora, Y. Yoshida, and G. Saito, J. Appl. Phys. **102**, 064913 (2007).
[7] K. Terhune and L. King, in *32nd International Electric Propulsion Conference, 11–15 September, Wiesbaden Germany, IEPC* (2011).
[8] P. Lozano and M. Martinez-Sanchez, J. Colloid Interface Sci. **282**, 415 (2005).
[9] D. G. Courtney and P. Lozano, Transact. Jpn. Soc. Aeronaut. Space Sci. **8**, 73 (2010).
[10] R. S. Legge and P. C. Lozano, J. Propul. Power **27**, 485 (2011).
[11] G. I. Taylor, Proc. R. Soc. London. Ser. A **280**, 383 (1964).
[12] M. Martinez-Sanchez, "Lecture 23–25: Colloidal engines. appendix", (2004).

[13] J. F. De La Mora and I. G. Loscertales, J. Fluid Mech. **260**, 155 (1994).
[14] Y.-H. Chiu, G. Gaeta, T. Heine, R. Dressler, and D. Levandier, in *42nd AIAA/ASME/SAE/ASEE Joint Propulsion Conference and Exhibit, Sacramento, CA, July 9–12, 2006* (AIAA, Sacramento, CA, 2006).
[15] Y.-H. Chiu, G. Gaeta, D. Levandier, R. Dressler, and J. Boatz, Int. J. Mass Spectrom. **265**, 146 (2007).
[16] M. Gamero-Castano and V. Hruby, J. Propul. Power **17**, 977 (2001).
[17] M. Gamero-Castano, Phys. Rev. Lett. **89**, 147602 (2002).
[18] S. P. Berg and J. L. Rovey, J. Propul. Power **29**, 339 (2013).
[19] J. Carretero and M. Martinez-Sanchez, Comput. Phys. Commun. **164**, 202 (2004).
[20] M. A. Herrada, J. M. López-Herrera, A. M. Gañán-Calvo, E. J. Vega, J. M. Montanero, and S. Popinet, Phys. Rev. E **86**, 026305 (2012).
[21] J. de Andrade, E. S. Boes, and H. Stassen, J. Phys. Chem. B **106**, 13344 (2002).
[22] J. W. Daily and M. M. Micci, J. Chem. Phys. **131**, 094501 (2009).
[23] N. Takahashi and P. C. Lozano, in *44th AIAA/ASME/SAE/ASEE Joint Propulsion Conference and Exhibit, Hartford, CT, July 21–23, 2008, AIAA-2008-4533* (AIAA, Hartford, CT, 2008).
[24] T. Coles and P. Lozano, in *49th AIAA/ASME/SAE/ASEE Joint Propulsion Conference and Exhibit, San Jose, CA, July 14–17, 2013* (AIAA, San Diego, CA, 2013).
[25] A. Borner, Z. Li, and D. Levin, J. Chem. Phys. **136**, 124507 (2012).
[26] A. Borner, Z. Li, and D. Levin, J. Phys. Chem. B **117**, 6768 (2013).
[27] A. Borner and D. Levin, IEEE Trans. Plasma Sci. (2014).
[28] C. Merlet, M. Salanne, and B. Rotenberg, J. Phys. Chem. C **116**, 7687 (2012).
[29] Y. Wang, S. Izvekov, T. Yan, and G. A. Voth, J. Phys. Chem. B **110**, 3564 (2006).
[30] Y. Wang, W. G. Noid, P. Liu, and G. A. Voth, Phys. Chem. Chem. Phys. **11**, 2002 (2009).
[31] C. Ryan, K. Smith, and J. Stark, Appl. Phys. Lett. **104**, 084101 (2014).
[32] W. J. Scheideler and C.-H. Chen, Appl. Phys. Lett. **104**, 024103 (2014).
[33] J. P. Stark, M. S. Alexander, and K. L. Smith, J. Appl. Phys. **115**, 044905 (2014).
[34] J. Carretero, F. Higuera, and M. Martinez-Sanchez, in *International Electric Propulsion Conference, Toulouse (Fr), Toulouse, France* (2003).
[35] J. Carretero, P. Lozano, and M. Martinez-Sanchez, in *4th International Spacecraft Propulsion Conference, Chia Laguna, Sardinia, Italy* (2004), Vol. 555, p. 106.
[36] J. A. Carretero Benignos, Ph.D. thesis, Massachusetts Institute of Technology, 2005.
[37] R. D. Branam and M. M. Micci, Nanosc. Microsc. Therm. **13**, 1 (2009).
[38] X.-J. Fan, N. Phan-Thien, N. T. Yong, and X. Diao, Phys. Fluids **14**, 1146 (2002).
[39] S. Adelman and J. Doll, J. Chem. Phys. **64**, 2375 (1976).
[40] I. Todorov, W. Smith, K. Trachenko, and M. Dove, J. Mater. Chem. **16**, 1911 (2006).
[41] Y. Saad and M. H. Schultz, SIAM J. Sci. Comput. **7**, 856 (1986).
[42] C. K. Birdsall and A. B. Langdon, *Plasma Physics via Computer Simulation* (CRC Press, Boca Raton, FL, 2004).
[43] D. Wolf, P. Keblinski, S. R. Phillpot, and J. Eggebrecht, J. Chem. Phys. **110**, 8254 (1999).
[44] R. Shi and Y. Wang, J. Phys. Chem. B **117**, 5102 (2013).